Solar Energy 278 (2024) 112764

Contents lists available at ScienceDirect

Solar Energy

journal homepage: www.elsevier.com/locate/solener

Experimental study and simulation of Hybrid-Active solar thermal cylindrical chamber for Citrus Hystrix leaves drying

M.A.A. Azmi [a], A.A. Razak [a,b,*], M.A.S.M. Tarminzi [a], A.F. Sharol [a], A.S.M. Yudin [a], Z.A.A. Majid [c]

[a] Faculty of Mechanical and Automotive Engineering Technology, Universiti Malaysia Pahang Al-Sultan Abdullah, Pekan, Pahang, Malaysia
[b] Centre for Advanced Industrial Technology (AIT), Faculty of Mechanical and Automotive Engineering Technology, Universiti Malaysia Pahang Al-Sultan Abdullah, Pekan, Pahang, Malaysia
[c] Kuliyyah of Allied Health Sciences, International Islamic University of Malaysia, Kuantan, Pahang, Malaysia

ARTICLE INFO

Keywords:
Hybrid dryer
Solar collector
Solar dryer
Citrus Hystrix leaves
Solar thermal

ABSTRACT

This article presents a study of a modular hybrid active solar drying system (MHASD) with parallel collector configuration for the dehydration process of the Citrus Hystrix plant in a cylindrical drying chamber. The system utilized a novel cylindrical drying chamber for solar and low temperature drying integrated into the MHASD system. The experiments were conducted outdoors and exposed to the external environment. The dryer performance was studied by measuring the heat recovered in the drying chamber, the moisture removal capacity, and the efficiency of the MHASD system based on the drying load of Citrus Hystrix sheets. The effectiveness of air flow and temperature distribution in the cylindrical drying chamber was investigated using the computational fluid dynamics (CFD) method. The air temperature in the drying chamber with the hybrid system reached 45 °C to 60 °C on a day with clear skies and variable weather. The drying time of the leaves was 6.5 h when collectors were used, while with the hybrid system it took 4 h to reach the final mass of 16 g. In intermittent weather conditions, the highest drying efficiency of 35.24 % was observed with the hybrid system, while drying with collectors was 17.26 %.

1. Introduction

Technological innovation encourages people to explore more energy sources for industrial processes. In 2030, there is an expected rise of more than 60 % of the world's energy demand, worsening climate damage, and increasing the security issue of energy supplyMoudakkar et al. [7]. Integrating solar thermal technologies into the industrial sector is a promising alternative to replacing fossil fuels since it is environmentally friendly and unlimited. More than 30 % of the energy produced worldwide is used in agriculture, with 3.6 % going toward dry biological wet goods[24].

The leaves of Citrus hystrix are known as one of the most aromatic herbs and are abundantly grown in Asian countries such as Laos, Indonesia, Malaysia, Vietnam, and Thailand. Citrus Hystrix leaves are known to bring many health benefits and are used in cooking. Leaves can help reduce headaches and gout and maintain our health care. Furthermore, cooking with Citrus Hystrix leaves is integral to Southeast Asian cuisine, especially in Thai dishes. Since fresh Citrus Hystrix has a short post-harvest life, they are dried and packed in plastic film before they are exported to other countries such as the United States of America, the United Kingdom, and Australia[13]. A fluidized bed dryer with inert sand particles was used to dry Citrus Hystrix leaves at 50 °C with different air velocities[22]. The findings demonstrated the surface air velocity and drying rate of Citrus Hystrix leaves [9]. The addition of inert particles to the dryer improved the drying process. Phoungchandang et al. [12] analyzed the drying process of Citrus Hystrix leaves using a heat pump-dehumidified and compared it with tray drying. The citronellal content was higher with the heat pump-dehumidified drying used because of the reduced drying time compared to tray drying.

Drying is one of the most determining post-harvest processes, as it discourages enzymatic degradation and microbial growth and preserves agricultural and marine products for longer periodsOliveira et al. [10,26] by reducing the moisture content of the products until it reached a safe limit to prevent the microorganism from spreading (S. [19]. Before modern technologies were widely applied in agriculture, drying activities were traditionally carried out in the open sun. Although this conventional method requires a lower investment cost, open-sun drying requires a large open space since the dried products must be spread to obtain radiation directly from the sun. The approach also causes a longer

* Corresponding author.
E-mail addresses: amirrazak@umpsa.edu.my, amirrazak@outlook.com (A.A. Razak).

https://doi.org/10.1016/j.solener.2024.112764
Received 19 February 2024; Received in revised form 30 May 2024; Accepted 9 July 2024
Available online 19 July 2024

Nomenclature

A	area (m^2)
C_p	specific heat capacity (kJ/kg K)
G	solar irradiance (W/m^2)
h_{fg}	latent heat of evaporation (J/kg)
$\dot{m}$	mass flow rate (kg/s)
P	pressure (Pa)
Pr	productivity of the system (kg)
Q	power gain (W)
T	temperature (^{0}C)
t	time (s)
$U_{.R.}$	uncertainty
V	volume flow rate (m^3/s)
v	velocity (m/s)
W	auxiliary heater power (W)
ρ	density (kg/m^3)
η	efficiency
ΔT	temperature difference (^{0}C)
σ	tolerance
Subscript	
a	air
c	collector
d	drying chamber
f	fluid
o	outlet
i	inlet

drying period since it is highly dependent on the availability of sunlight. There is a high possibility of producing low-quality products that thrive in moist conditions. Therefore, a solar drying system could be an excellent alternative to replace open sun drying.

Solar drying can be classified into four main groups: open sun drying, direct solar drying, indirect solar drying, and hybrid solar drying[6]. They can be divided by distinguishing the solar thermal componentsHao and Shuonan Liu [27]. [18] innovated a technique to improve the thermal performance of a direct solar dryer by using a geothermal water heat exchanger as an additional heat source. The findings showed that the installation of a heat exchanger improved the performance of the solar dryer. The lowest recorded temperature was 46° C, while the highest was 58° C. Installing a heat exchanger provides continuous drying at night or on cloudy days. [11] investigated an indirect solar dryer by evaluating the dryer's characteristics and the effect on sweet cherry drying. The authors concluded that the solar dryer was less energy-intensive and affordable. The electrical heating cost was less than 5 %, and the indirect forced solar dryer also did not significantly impact the quality of sweet cherry fruit, resulting in a more efficient drying process than open sun drying. [5] presented a study on indirect grape drying. The heat transfer from the water storage tank kept the grapes' temperature higher than the ambient temperature during the intermittent solar radiation conditions. The initial moisture content was 79.8 % (w.b.) and was reduced by 20.2 % (w.b.) in 120 h of indirect solar drying and 201 h during open sun drying, respectively. [2] conducted experiments and a numerical method to analyze the efficiency of cylindrical-type drying chambers developed, increasing the drying performance and time from 3.03 to 1.73 and 3.07 to 1.77. Bhavsar and Patel [31] used a cabinet-type dryer with more capacity, in which the efficiency can be increased beyond 3 % by using the dryer's thermal energy storage material efficiency.

In order to overcome the insufficient heat supplied to the solar dryer,

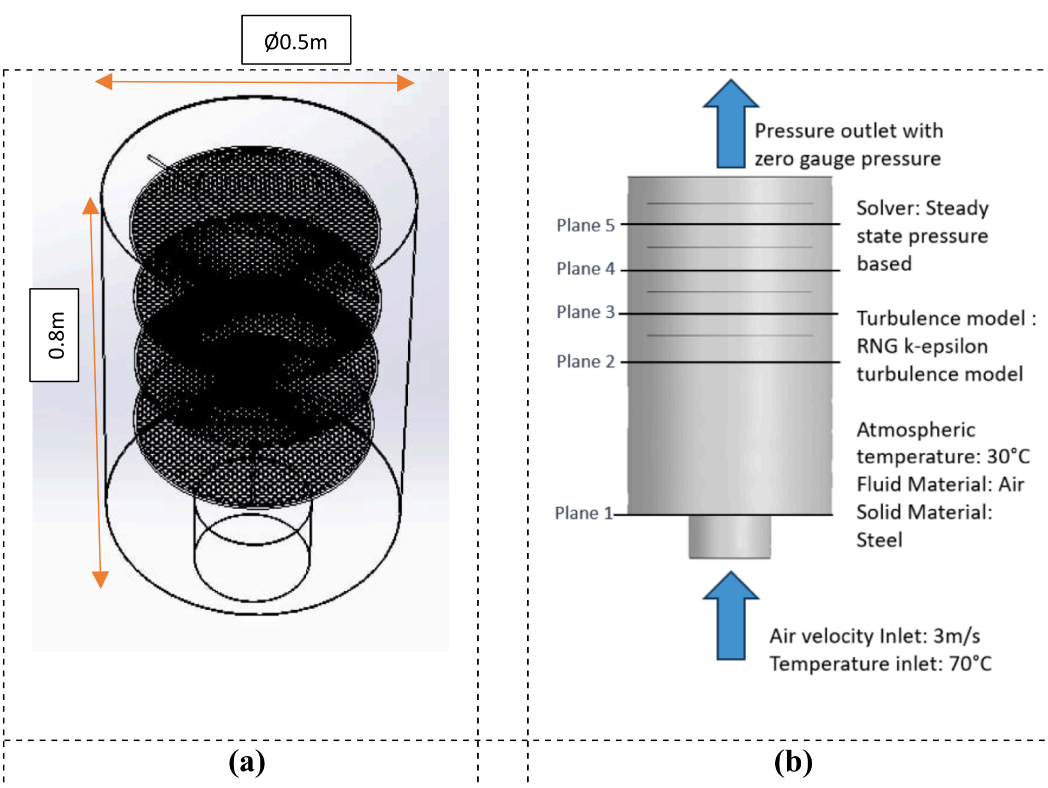

Fig. 1. Details of the cylindrical solar drying chamber: (a) design geometry; (b) boundary condition.

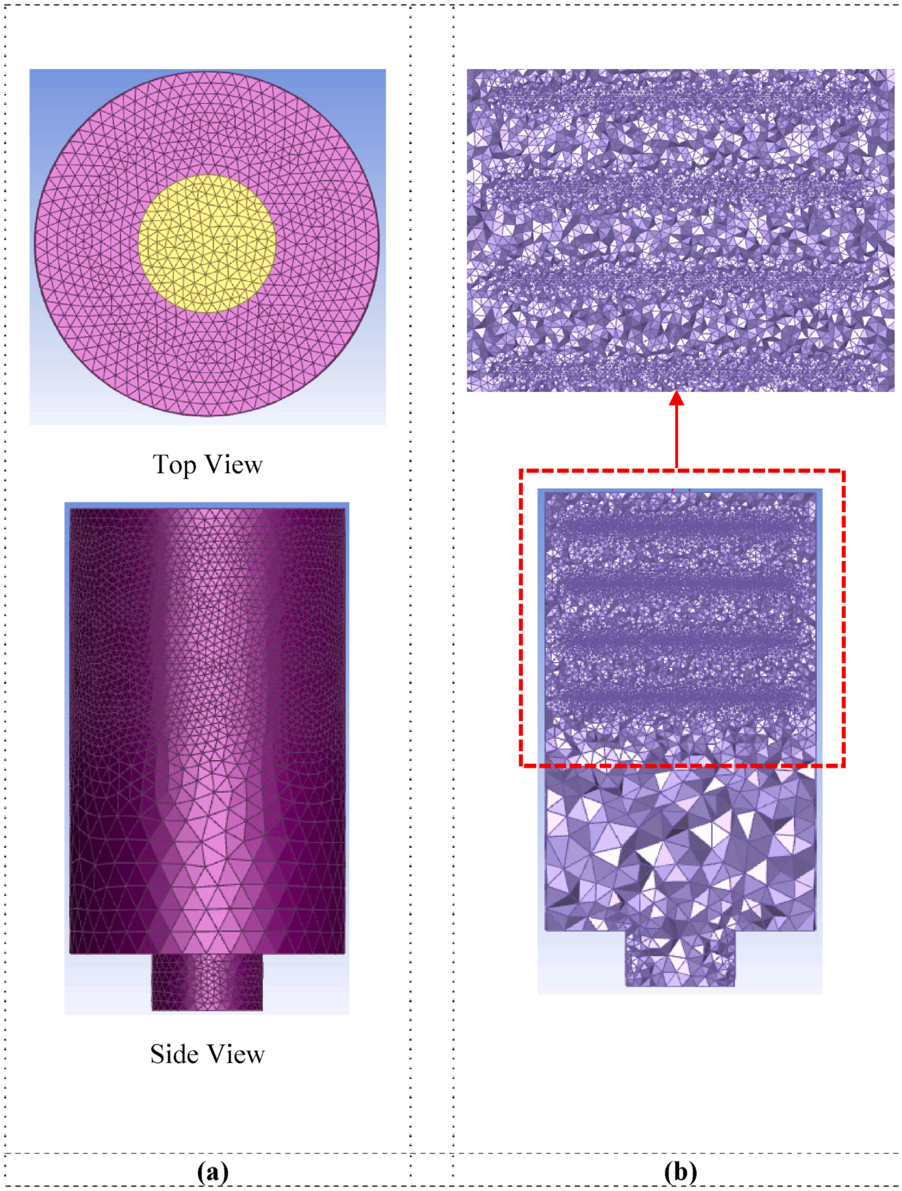

Fig. 2. Meshing structure of cylindrical drying chamber: (a) Side view with enlarged top view of inflation region; (b) Meshing structure volume mesh cut section near tray section layers.

a hybrid element can be added to the drying system. Suherman [20], developed a hybrid drying system with an auxiliary thermal source. Coffee beans were used as the target product and the results showed that drying was faster, with a collector efficiency of 54.15 % compared to the solar process of 50.07 %. To construct a prototype hybrid solar thermal drying system, Yassen and Al-kayiem [28] employed a hybrid dryer with an additional recovery dryer that increased to 13 % from 10.3 % when using hybrid drying without recovery.

This paper discussed the drying process of Citrus Hystrix leaves using a hybrid-active solar drying system in a parallel solar collector mode and a cylindrical type of drying chamber. The MHASD system consists of 4 components: solar collectors with cross-matrix absorbers, a mixing chamber, a novel (low-temperature drying) cylindrical drying chamber, and an auxiliary heater element as the hybrid element. Four layers of the tray are placed in the drying chamber to place fresh Citrus Hystrix leaves until dry. The solar dryer can operate in any weather since the drying temperature within the drying chamber can be adjusted with the help of an auxiliary heater. The solar dryers are compared to the system operation with and without an auxiliary heater.

2. Materials and methods

2.1. Simulation setup of cylindrical drying chamber

The CFD approach was used to assess the thermal energy and temperature distribution of the drying chamber. In addition to theoretical calculations, the simulation analysis used in this work is helpful to offer a better comparison between the outcomes. Ansys Fluent software was used as a CFD tool in the simulation study for this work to evaluate the behavior of the airflow and temperature distribution in the drying chamber, Al-Kayiem and Gitan [29]. A novel cylindrical design for the MHASD system was developed to improve its performance. The initial phase involved designing and simulating a cylindrical solar drying chamber. The primary goal of this simulation is to evaluate the airflow efficiency and temperature distribution by examining the contours of the velocity and temperature results.

Furthermore, because of the cylindrical shape of the drying chamber's extension residence period of air inside, these configurations allow the chamber to increase the time and collect more hot airflow. The Ansys

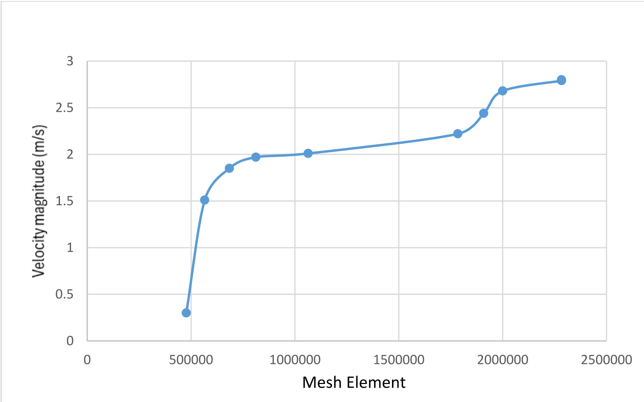

Fig. 3. Mesh independent study of the velocity magnitude against the mesh element in the mesh tray area.

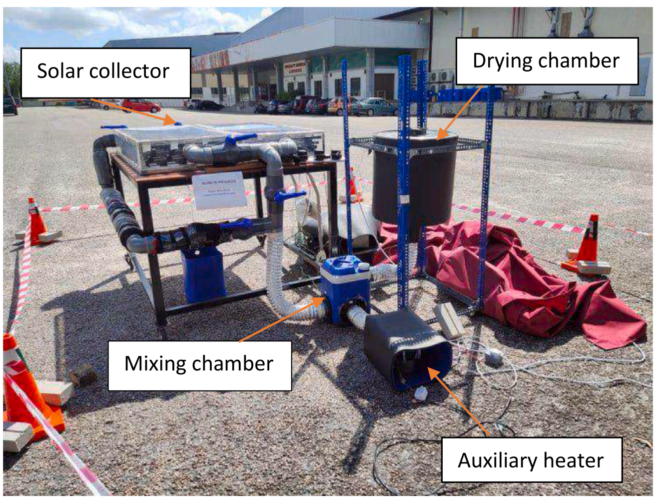

Fig. 4a. Setup for solar drying system.

Fluent Geometry module was used to develop the system's geometry. Fig. 1(a) and (b) depict the geometry of the cylindrical drying chamber design and the boundary conditions. Aluminum material is used for better heat conductivity. Fig. 2 shows the mesh created for the chamber with 2,286,537 elements. The comparison graph of the velocity magnitude at different mesh levels was chosen as shown in Fig. 3; the chosen mesh level range is because it has a stable convergence and a smooth curve compared to other meshes. In order to ensure that the CFD modeling is in a condition similar to the experimental work, the working fluid domain was modeled as air at room temperature and entered into the plenum chamber with known specific pressure. The inlet static pressure was measured experimentally and used as boundary input for the simulation. The initial gauge pressure at the outlet boundary was assumed to be 0 Pa for initialization. The non-slip boundary condition was applied to the remaining solid boundaries. Enhanced wall function was used in the input region and throughout the solar drying chamber wall. The Re-Normalization Group (RNG) $k - \varepsilon$ model was used in this study since it is a widely used turbulence model for the solution of practical engineering flow problems [30]; Liu & Bai, 2015 and Sergioet al, 2011).

2.2. Experimental setup

The hybrid solar dryer consists of four main components: double solar collectors, a drying chamber, a mixing chamber, and one heating element, as shown in Fig. 4(a), with the schematic diagram of the setup in Fig. 4(b). Designing a thermal absorber and choosing suitable coatings are essential for effectively harvesting solar energy[25]. A pair of cross-matrix absorber solar air collectors was used during the experiment. It has the ability to produce higher energy gains compared to the flat-plate solar air collector[32]. A flat black spray was applied to the absorbers to prevent heat reflection and maximize heat absorption. The assembly of the solar dryer design is illustrated in Table 1:

The geometrical layout of the drying chamber offers the benefit of achieving an even distribution of airflow around the dried goods. Furthermore, it is very effective in drying lightweight herbs[1] as drying occurs in a closed environment, preventing dried products from escaping due to airflow. A four-layer tray was used to place the Citrus Hystrix leaves inside the drying chamber, as shown in Fig. 5. Citrus Hystrix leaves were obtained from the market and kept in the refrigerator for one night at temperatures ranging from about 2 °C to 5 °C to ensure freshness, as experiments were carried out early in the morning. The experiments were conducted from 9 am to 5 pm at Universiti Malaysia Pahang, Malaysia. 260 g of leaves were weighed, 65 g of Citrus Hystrix leaves were placed on four layers of the tray and the arrangement of leaves was set into three groups at each thermocouple location. The leaves are weighed at 30 min interval until they reach their equilibrium mass.

2.3. Evaluating the performances of MHASDS

The solar dryer was tested by drying Citrus Hystrix leaves without the hybrid system and then comparing the results with the hybrid system during clear skies and intermittent weather conditions. Ventilation fans were set at 2 m/s for all three tests to transfer heated air to the drying chamber. The experiments were carried out for 8 h, from 9 am to 5 pm. Radiation and ambient temperature in the system are measured using a pyranometer and K-type thermocouples. Fig. 6 shows that the collectors in series arrangement required a longer distance for air to move from collector 1, collector 2, the mixing chamber, and the drying chamber. Although a higher air temperature was achieved at the outlet of collector 2 for the series configuration, a more significant heat loss occurred. The long air travel distance from the collector to the drying chamber increases the chance of heat losses due to conduction [23]. More air particles collide and heat transfer activity occurs, leading to a lower air temperature gain in the drying chamber. Although the 20 mm thick insulator was mounted on the surface area of the conduit to reduce heat escaping into the environment, much heat remained lost. The maximum air temperature achieved inside the drying chamber for the parallel arrangement was 4 °C higher than the series arrangement when the air velocity was increased to 2 m/s. Therefore, a parallel collector configuration was used since it reduced the air travel distance from the collector to the drying chamber[33]. A higher air velocity was also required to minimize potential heat losses to the environment and provide maximum heated air in the drying chamber, especially in a case with a long air travel path.

2.4. Thermal analysis

The power gained in this section was analyzed on the basis of the first law of thermodynamics. The power balance during the experiment was presented in Eq. (1):

$$\dot{Q}_A = \dot{Q}_u + \dot{Q}_{loss} \tag{1}$$

where $\dot{Q}_A$, $\dot{Q}_u$ and $\dot{Q}_{loss}$ were the energy absorbed, useful and loss.

The $\dot{Q}_A$ which the power gained by the collector can be expressed in Eq. (2) below:

$$\dot{Q}_A = A_c G \tag{2}$$

The power gain in the system involves the mass flow rate of air, the specific heat capacity of the air, and also the temperature difference

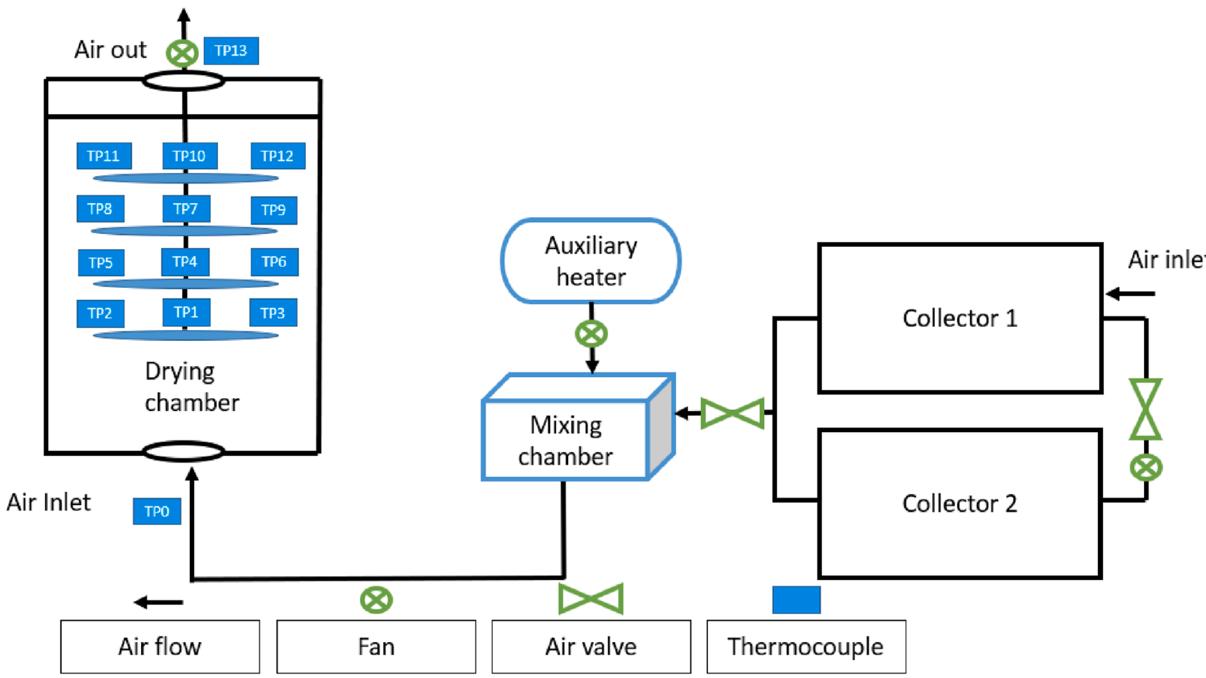

Fig. 4b. Schematic diagram of the experimental setup of the solar drying system.

Table 1
Detail of the solar dryer system.

Collectors (unit)	2
Material (absorber)	Square tube Aluminium
Type (absorber)	Cross-matrix absorber
Dimension (absorber)	1.12 m X 0.59 *m*
Aperture area	1.219 m^2
Working fluid	Air
Insulation material	Insulfex® closed-cell elastomeric nitrile rubber foam with thickness of 20 mm
Material (cover plate)	Polycarbonate
Ventilation fan (unit)	4
Ventilation fan (specifications)	12 V DC, 0.55A
Material (drying chamber)	Stainless steel
Dimension (drying chamber)	50 cm x 80 cm
Auxiliary heater (specification)	300 W 220 V AC heater

between the inlet and outlet of the solar collector. The air passing through each collector undergoes convection with the absorber to produce heat that is transferred into the drying chamber. The power balance can be presented by the following equation:

$$\dot{Q}_u = \dot{m}_a C_{pa}(T_o - T_i) \tag{3}$$

The mass flow rate was calculated by measuring the velocity of the air across the collector and using the following expression (4):

$$\dot{m}_a = \rho_a A v_a \tag{4}$$

Since the system is in steady flow with one inlet and one outlet, the mass flow rate of the air into and out of the control volume is identical where:

$$\dot{m}_{in} = \dot{m}_{cv} = \dot{m}_{out} \tag{5}$$

The initial and final phases inside the drying chamber are all factors that affect the increase in energy of the system. The air supplied from the ambient passes through solar collectors, which are heated through convective heat transfer between the heated absorber and the air. The heated air is then transferred into the drying chamber through ducts that connect both components. The following equation presents the energy transfer:

$$\dot{Q} = \rho_f A v_f C_{pf}(T_{final} - T_{initial}) \tag{6}$$

The difference between the initial and final temperatures of the drying chamber determines how much energy is used. ρ_f and C_{pf}, respectively. It is assumed that the fluid density, ρ_f and specific heat capacity, C_{pf} remain constant at 1.1 kg/m^3 and 1007 J/kg·K, respectively. (Cengel & Boles, 2002). Equation (3) is applicable in the low air temperature range between 40–60 °C and at a pressure of 1 atm.

2.5. Moisture content measurement

The fraction of moisture content (X) of Citrus Hystrix is calculated using Eq. (7) [21]and the effective diffusion coefficientCorrêa et al. [4]

$$X = \frac{m_t - m_k}{m_k}[gg^{-1}] \tag{7}$$

Where m_t is the weight of the wet Citrus Hystrix leaves (g) and m_k is the dry weight sample (g), with the unit of gg^{-1}.

The moisture ratio (M.R.) is calculated in Citrus Hystrix using Equation (8) [22].

$$MR = \frac{X - X_{eq}}{X_0 - X_{eq}}[\text{no unit, d.b}] \tag{8}$$

Where X_0 is the initial moisture content and X_{eq} is the equilibrium moisture content. However, since the value for X_{eq} is relatively small compared to X and X_0, it is negligible [3,14]. Therefore, Eq. (9) can be simplified to Eq. (6).

$$MR = \frac{X}{X_0} \tag{9}$$

The drying rate can be calculated using Eq. (10):

$$DR = \frac{X_{t+dt} - X_t}{dt}[gg^{-1}h^{-1}] \tag{10}$$

where dt is the time interval.

Fig. 5. Photographs of Citrus Hystrix leaves (a) side view 4 layer mesh trays; (b) top view 4 layer mesh trays.

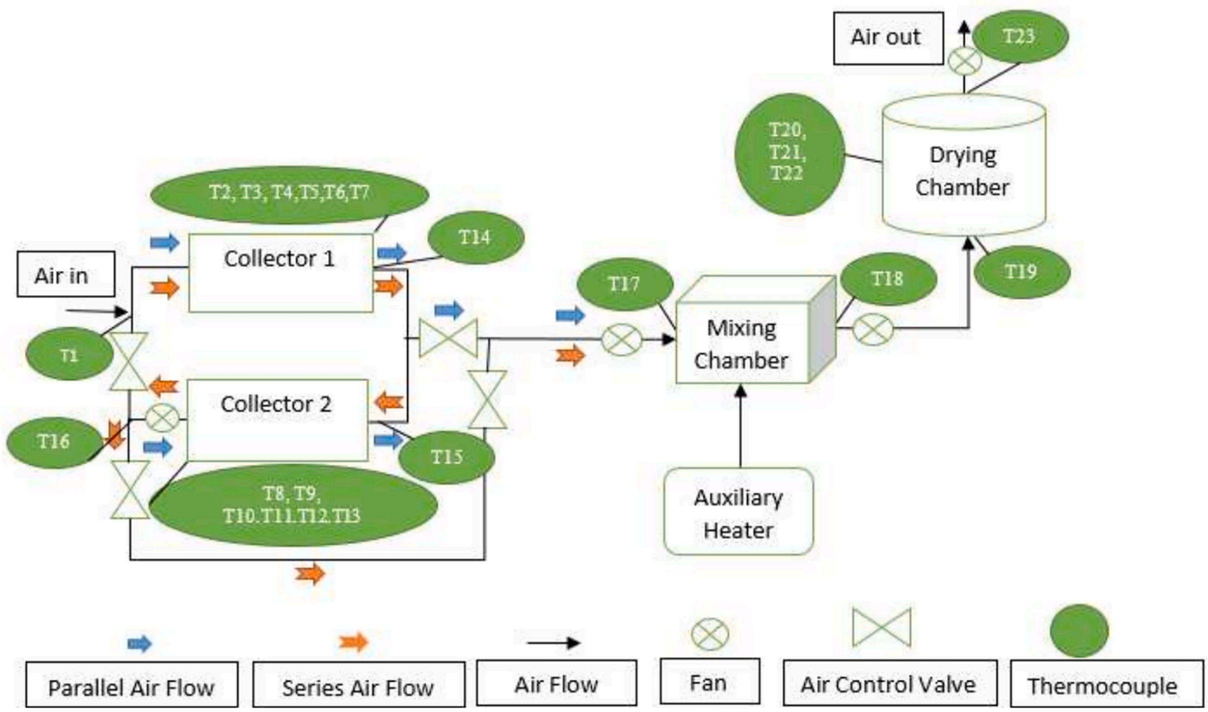

Fig. 6. Air flow direction for collector arrangement configuration.

2.6. Solar dryer efficiency

By dividing the output of each component of the system by its input, the efficiency is calculated. The efficiency of the collector can be said in the following way:

$$\eta_{col} = \frac{\dot{Q}_a}{GA_{col}} = \frac{\dot{V}.\rho_a.\Delta T.C_{pa}}{G.A_{col}} \tag{11}$$

The efficiency of the drying chamber is shown by the following equation.

$$\eta_d = \frac{Pr.h_{fg}}{(G.A_{coll} + W)t} \tag{12}$$

Here Pr the productivity of the system (kg), h_fglatent heat of evaporation (J/kg), G the solar irradiance (W/m2), A_c area of collector (m2) and W the auxiliary heater power (W).

Table 2
Accuracy of measuring instruments.

Instruments	Quantity	Accuracy
K-type thermocouple	23	−1.5 °C to + 1.5 °C
Pyranometer	1	0.1 W/m^2

Table 3
Parameters of uncertainty.

Description	Unit	Uncertainty	Relative uncertainty (%)
Ambient temperature	° C	±0.10	0.48
Internal temperature	° C	±0.10	0.72
Ambient temperature	° C	±0.10	0.48
Solar radiation	W/m^2	±12	2.04

For the heater, the efficiency is calculated as follows:

$$\eta_h = \frac{\dot{m}.C_p.\Delta T}{I.V} \tag{13}$$

The overall efficiency of the system:

$$\eta_{overall} = \eta_{col} X \eta_d X \eta_h \tag{14}$$

2.7. Uncertainty analysis

The measurements performed were subject to uncertainties, which are elaborated on in this section. The accuracy of each instrument used was determined and presented in Table 2, while the parameters that are studied in this article involve uncertainty were shown in Table 3 based on the previous study by [15] and (Ahmad Fadzil [16].

Every x_n, the measurements have the measurement tolerance of σ_n, and the uncertainty of the measurement parameters, $U_{.R.}$, can be calculated by using Equation (12)(A. F. [17]:

$$U_R = \left\{ \left(\frac{U_R}{dx_1}.\sigma_1 \right)^2 + \left(\frac{U_R}{dx_2}.\sigma_2 \right)^2 + \left(\frac{U_R}{dx_3}.\sigma_3 \right)^2 + \cdots \left(\frac{U_R}{dx_n}.\sigma_n \right)^2 \right\}^{\frac{1}{2}} \tag{12}$$

Based on Equation (12), the uncertainty of the power gained by the system was 314.14 ± 7.68 W with a relative uncertainty of 2.45 %, respectively, on sunny 25 January 2020.

3. Results

3.1. Simulation result

To analyze the flow pattern at different locations within the drying chamber, five horizontal planes (X-Z) were made at y = 0.05, 0.4, 0.5, 0.6, 0.7 m, were made through the 3D fluid domain. The description of flow dynamics inside the drying chamber is discussed by analyzing the velocity contours and velocity streamlines of different computational fluid domains. The flow patterns within the drying chamber were heterogeneous in the cylindrical solar drying chamber design. The airflow inside the drying chamber was spread uniformly as the heated air flow passed through to the chamber's intake. Interestingly, the cylindrical shape of the drying chamber affected air mobility by improving the eradication of large dead zone regions. A numerical analysis of the cylindrical drying chamber was performed to investigate the effects of airflow and temperature distribution. To illustrate the velocity distribution in the air domain of the cylindrical drying chamber, a 3D contour and velocity streamlines are shown in Fig. 7.

The cylindrical drying chamber velocity contour in Fig. 7 demonstrates that the air velocity peaked at two positions. The first is near the hole's inlet, and the second is near the drying chamber's outlet. The low-pressure suction fan at the solar drying chamber outlet provides advantages in airflow rate distribution. As a result, the blow and suction of the pressurized fan blower have significantly reduced the area of the dead zone region at the bottom of the chamber. The contours show a distinct and uniform airflow was dispersed throughout the drying chamber. At a constant air velocity of 3.0 m/s, airflow behavior in a cylindrical drying chamber was investigated.

The vertical and horizontal planes shown in Fig. 8, along with the efficiency of the drying chamber, were evaluated using a cylindrical drying chamber in terms of temperature distribution. The interior temperature distribution of the cylindrical drying chamber is increasing and becoming more uniform as the air velocity increases. According to the results, cylindrical drying chambers have an advantage over other types, since they can capture a higher percentage of thermal energy while extending the air.

3.2. Experimental result

To see the significant temperature difference between the numerical simulation and the actual experimental results more intuitively, the drying chamber was divided into two cross-sectional areas section A and B according to the distribution of the digital thermocouple, namely TP1 to TP12 in the meshing tray area, as shown in Fig. 9. Since there was little difference in temperature at the symmetrical planes of the cross-section, six points on one side of the cross-section were selected for temperature testing in each area. Fig. 10 is a comparison diagram of the numerical simulation and experimental results of the maximum temperature in the drying chamber at section A and section B. It can be seen that although the maximum temperature measured at each point of the simulation results was higher than the actual experimental results, the overall trend and posture of the simulation results were similar to the actual experimental results. Especially at TP3, TP4, TP5, and TP6, the difference between the numerical simulation and the experiment was small. It can be seen that the maximum temperatures of the points in the two cross-sectional areas A and B were quite different. Regardless of the conditions of Section B near the outlet of the drying chamber, the maximum temperature of TP7 to TP12 was lower than TP1 to TP6 and there was a certain temperature difference between TP9, TP10 and TP11. Therefore, it can be explained that the temperature distribution near the inlet air distribution of the drying chamber differed greatly in the radial direction, and the degree of temperature change gradually decreased with the change of section.

The solar radiation and the temperature changes inside the drying chamber during the outdoor drying process are shown in Fig. 11. There are two sets of controls, one with the solar collector as the sole heat source (Fig. 11a), while the other set of controls (Fig. 11b) uses hybrid heat sources (solar collector and electric auxiliary heater). Each experiment used 260 g of Citrus Hystrix leaves and dried for 8 h from 9 am to 5 pm. Atmospheric parameters were recorded. Solar radiation ranged from 236 W/m^2 to 1308 W/m^2, while the average ambient temperature during the experiments was 27.3 °C. The data showed that the air temperature recorded inside the drying chamber varied from 32° C to 60° C. Compared to open air sun drying, the air temperature within the drying chamber was higher at 30° C than the ambient air temperature. Both readings were taken on 25 January 2020 (sunny) and 26 January 2020 (intermittent) at the Universiti Malaysia Pahang Al-Sultan Abdullah, Gambang, Pahang, Malaysia.

In Fig. 11a, it was observed that the air temperature inside the drying chamber changed linearly with solar radiation. The solar collector generates heat for the solar dryer, which depends on the intensity of solar radiation. Initially (from 9 am to 10 am), the drying chamber temperature was elevated at a slower rate because the energy received was used to heat the solar collectors. After 10 am, the temperature of the heated air supplied to the drying chamber is directly related to the energy absorbed by the collectors and the ambient temperature. The highest air temperature in the drying chamber was 56.37 °C, around 1 pm when the maximum solar radiation recorded was 1254.4 W/m^2.

For the hybrid system, as in Fig. 11b, a rapid increase of 22° C in the

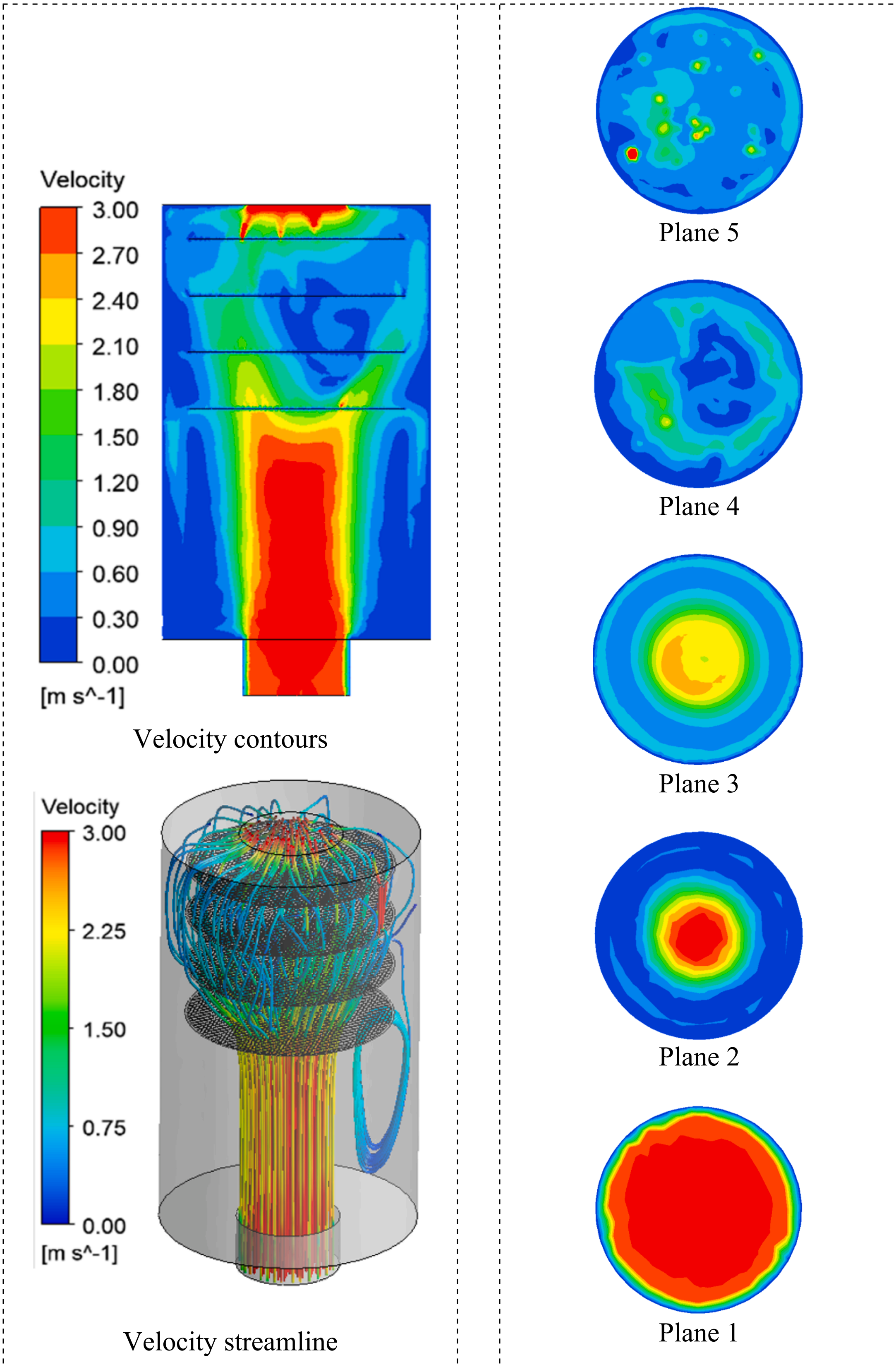

Fig. 7. Combined velocity contours and velocity streamlines of a cylindrical solar drying chamber.

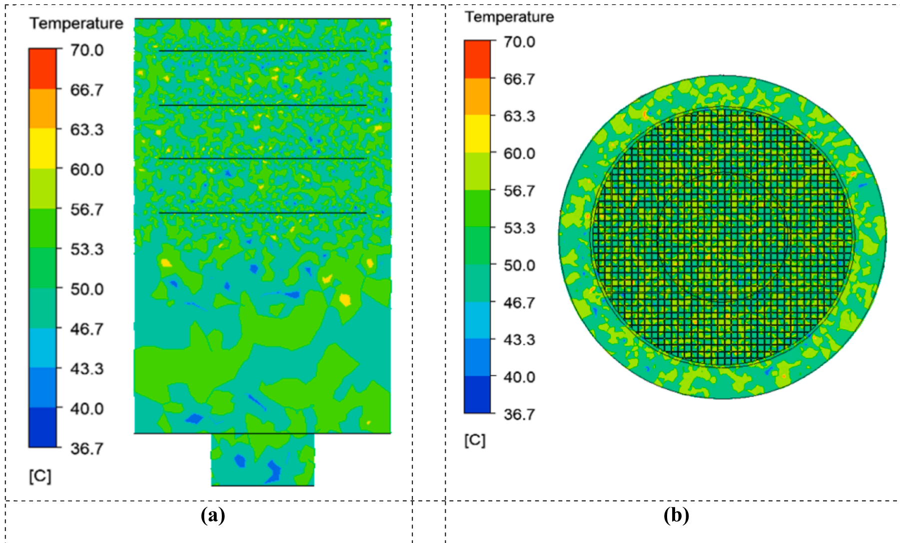

Fig. 8. Temperature contour: (a) vertical plane; (b) horizontal plane.

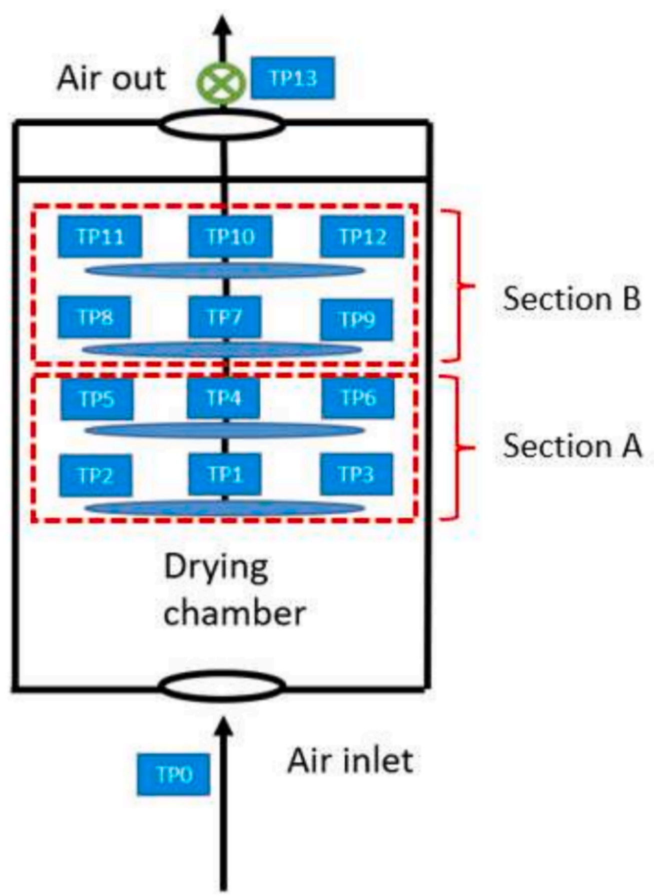

Fig. 9. Meshing tray regional division of drying chamber.

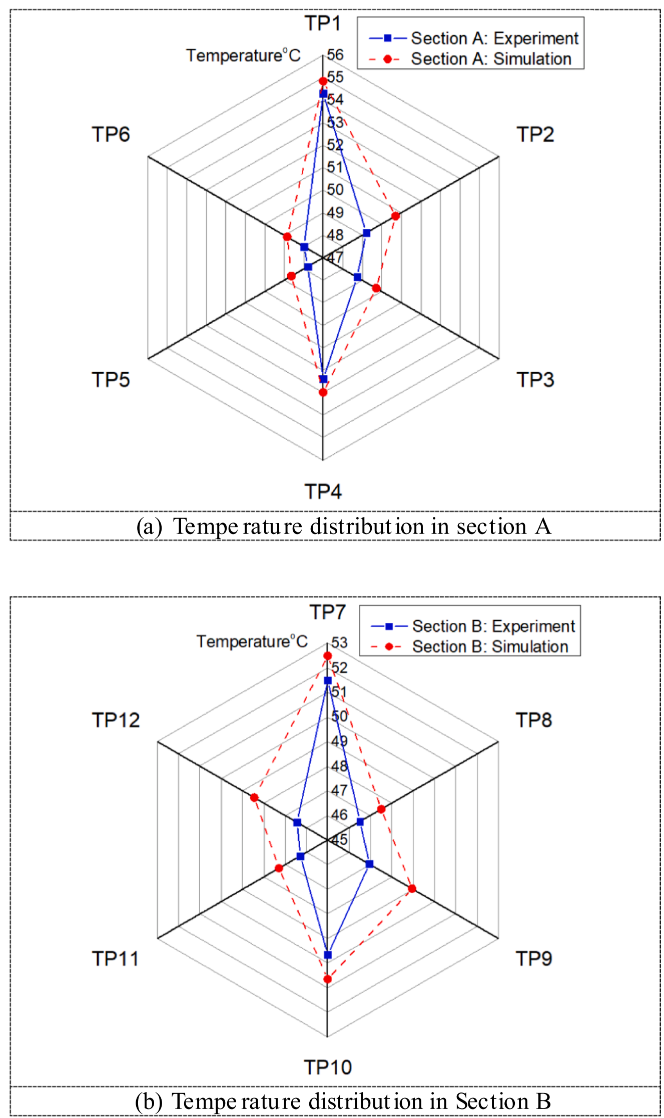

Fig. 10. Comparison chart of temperature distribution differences.

air temperature inside the drying chamber was recorded from 9 am to 11 am. Air inside the drying chamber could reach a maximum temperature of 60° C at 11.30 am before drying using the solar collector, since the auxiliary heater provided additional heat energy to the air inside the mixing chamber before the heated air entered the drying chamber. After 3 am, the drying temperature inside the chamber remained at 45° C to 53° C, although solar radiation decreased (from 510 W/m^2 to 480 W/

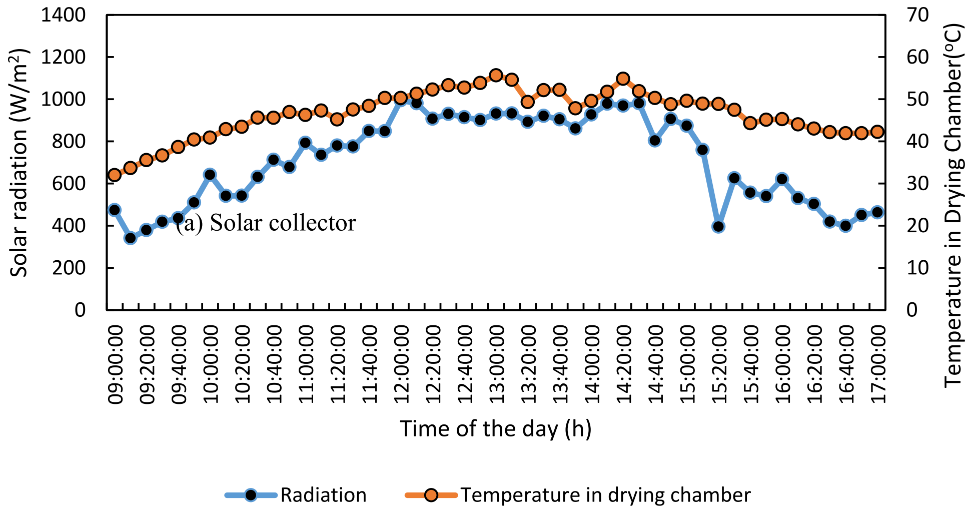

(a)

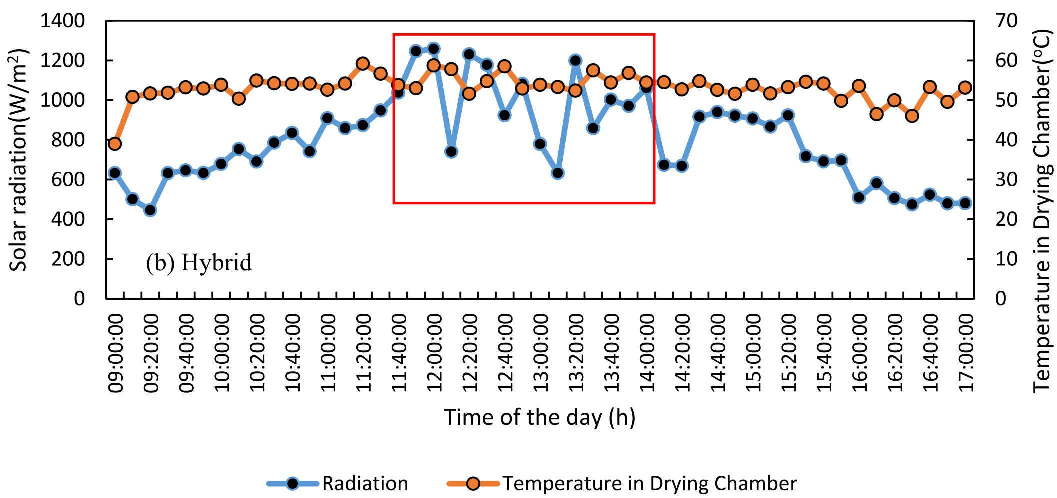

(b)

Fig. 11. The drying chamber temperature profile with (a) a solar collector and (b) a hybrid system.

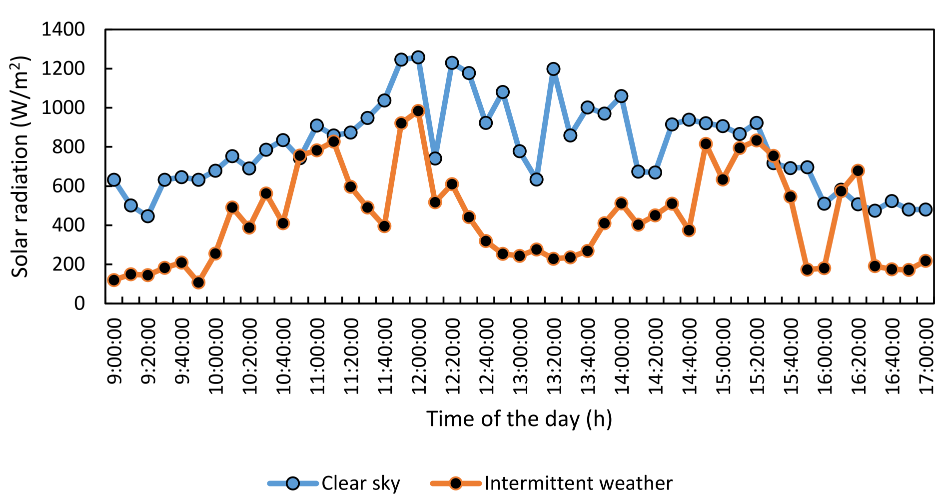

Fig. 12. Variations in solar radiation during drying on a clear-sky day and intermittent weather on 27 January 2020 and 7 February 2020.

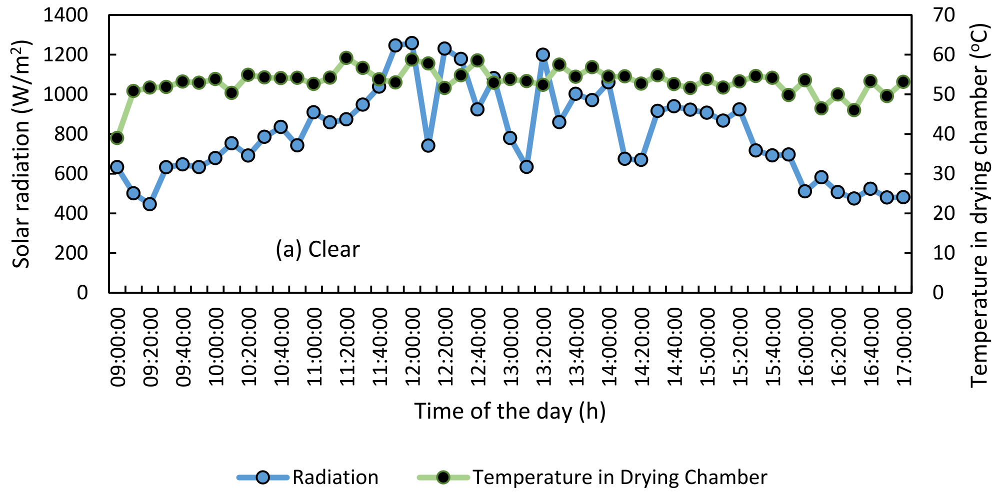

(a)

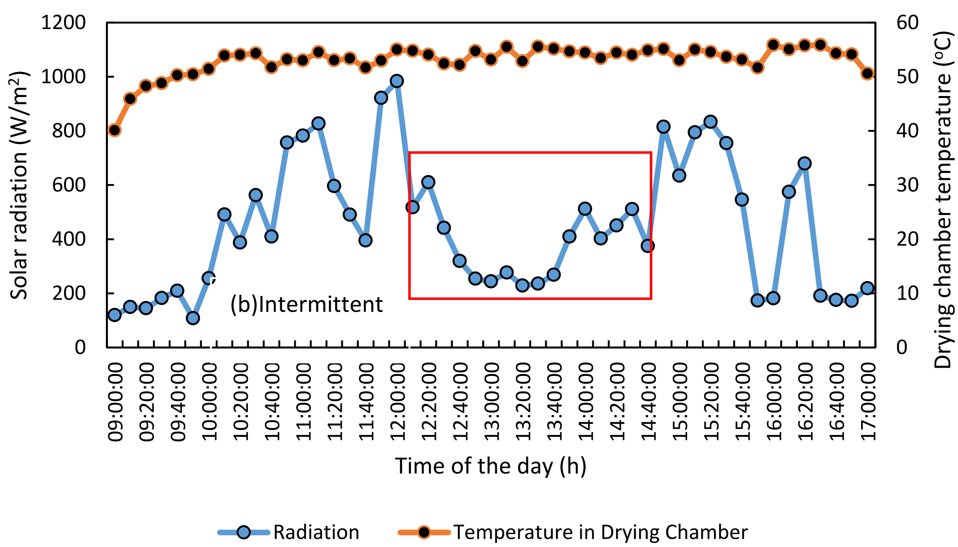

(b)

Fig.13. The drying chamber temperature profile during (a) clear skies and (b) intermittent weather.

m^2). The electrical heater was on for 2 h and consumed 0.995kWh

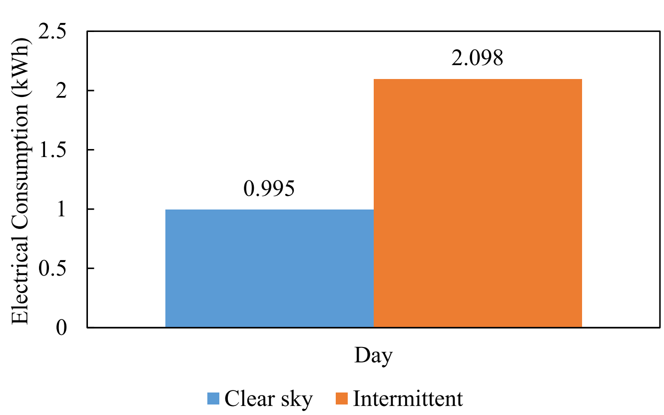

Fig. 14. Electricity consumption by the auxiliary heater during the experiments.

electrical power to supply additional heat to the system. Using the solar collector and the auxiliary heater, the hybrid drying system was able to maintain an ideal air temperature for the drying process, although the ambient temperature fluctuated as presented from 11.30 am to 2.30 am compared to drying using the solar collector alone, which relies on solar radiation from the Sun to produce heat.

The variation of solar radiation during two different weather conditions, clear skies and intermittent weather, is presented in Fig. 12. Both data were taken on a clear sky day and intermittent weather during hybrid solar drying of 260 g Citrus Hystrix leaves. The ambient temperature ranged from 20° C to 30° C. It was observed that solar radiation during clear sky days was higher compared to intermittent weather, especially during the afternoon between 12 am and 2 am.

The relationship between solar radiation and the increase in temperature inside the drying chamber is shown in Fig. 13. The average air temperature inside the drying chamber on a clear day was 53.39 °C, while during intermittent weather, the temperature was 53.47 °C. For both days, the temperature inside the drying chamber was retained

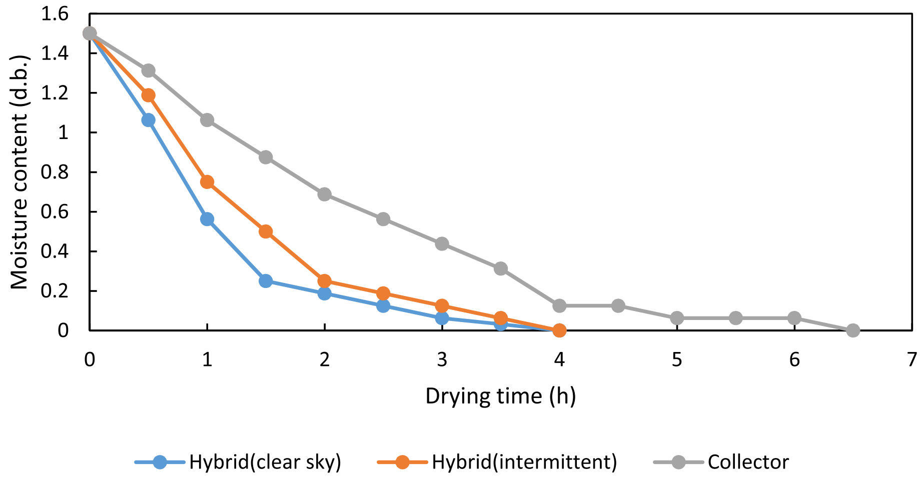

Fig.15. Drying curve of Citrus Hystrix leaves using a solar collector on clear sky (hybrid) and intermittent weather (hybrid) days.

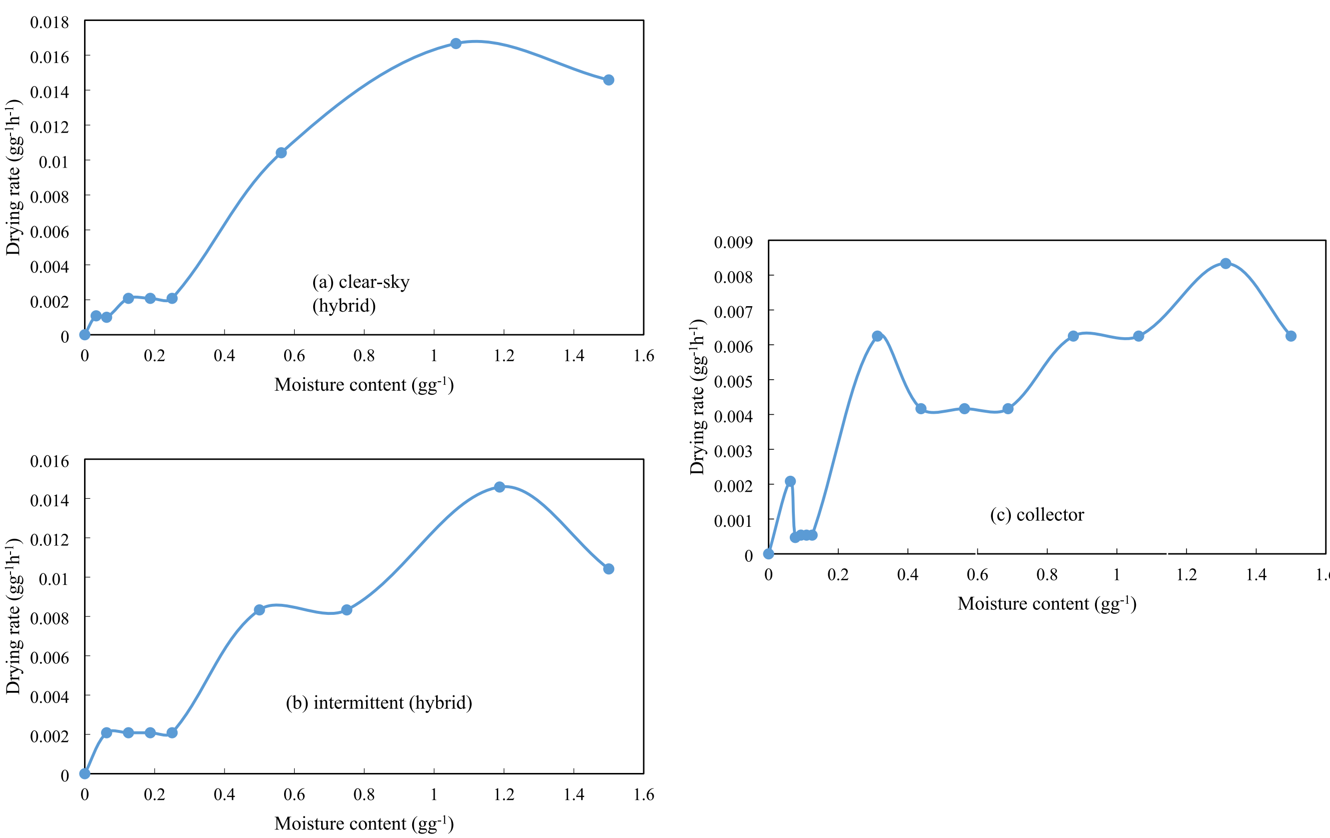

Fig.16. Drying rate of Citrus Hystrix leaves during (a) clear sky hybrid, (b) intermittent weather hybrid, and (c) collector.

between 45° C and 60° C, although the intensity of solar radiation, the primary heat source, was relatively low, particularly during intermittent weather. It can be seen in Fig. 13b that from 12 pm to 2.30 pm, the intensity of solar radiation was very low due to intermittent weather conditions. Additional warm air was supplied to the drying chamber by integrating the hybrid system into the solar dryer. A temperature controller regulates the air temperature within the drying chamber via responses from thermocouples and an electrical ceramic heater installed at the chamber's inlet. The auxiliary heater provides additional heat and is automatically turned off when the temperature reaches 60° C. This provides a uniform temperature distribution for drying Citrus Hystrix leaves, as the air temperature was maintained even though the solar collector produced low heat energy due to low solar radiation, especially during intermittent weather.

The electrical power consumption of the electrical heater was monitored using a digital power meter during the experiments, and the values are presented in Fig. 14. From the results, the power consumed by the heater in intermittent weather doubled compared to the day of clear skies. The electrical heater was turned on for 2 h and consumed electrical power of 0.995 kWh to supply additional heat to the system during the day of clear skies, while it was on for 4 h during intermittent weather with an electrical power consumption of 2.098 kWh. Since the solar radiation on the clear sky day was high, the collectors could produce the required heat energy to warm the air. This decreases the dependence on the auxiliary heater compared to the experiment during intermittent weather, where the heater was used more frequently to maintain the

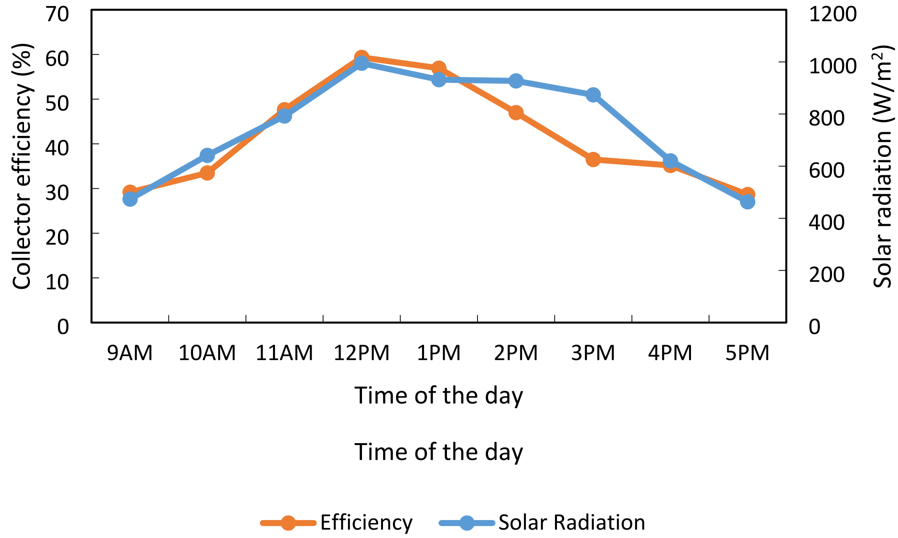

(a)

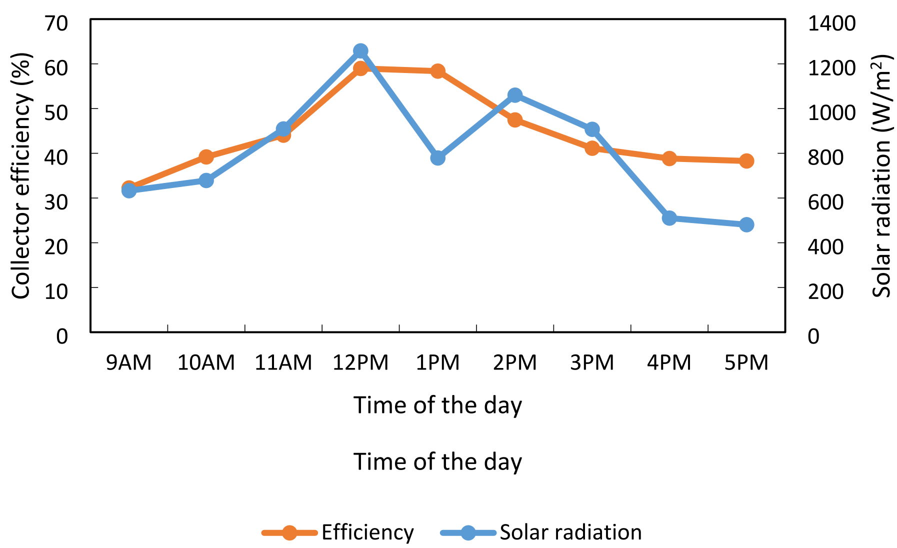

(b)

Fig. 17. Instantaneous efficiency of the solar collector during the drying of Citrus Hystrix leaves under outdoor conditions: (a) use of the collector; (b) hybrid on clear sky day; (c) hybrid in intermittent weather.

desired air temperature inside the drying chamber.

Fig. 15 shows the results of the drying curves for all three tests. Data were collected at a 30-minute interval until Citrus Hystrix leaves reached an equilibrium moisture content of 1.5 d.b. The 4-hour drying period for the hybrid system was observed to have clear-sky and intermittent weather. A drying system with a solar collector takes only 6.5 h to dry. The drying time was reduced by 38.46 % using the hybrid system compared to the collector-only drying system.

Meanwhile, the Citrus Hystrix leaves that are being dried by the collector drying system rely only on the performance of solar radiation. For the hybrid drying system, only 4 h were needed to dry the Citrus Hystrix leaves, although the weather changed. The auxiliary heater raises the temperature of the feed air from the solar collector before entering the drying chamber, ensuring a consistent ideal air temperature during the drying process.

The experimental results of the Citrus Hystrix leaves are shown in Fig. 16. The findings show that the Citrus Hystrix leaves dried more quickly in the beginning phases. The heat of the feed air that traveled through the meshing trays helped to evaporate the moisture from the surface of the leaves. As the drying process progressed, the drying speed slowed, reducing the amount of moisture that evaporated into the environment.

Fig. 16(a) and (b) showed similar patterns, as both used hybrid elements. In contrast to Fig. 16c, the solar collector's heat source is based on solar radiation, which, in this case, fluctuates. As a result, the moisture removal rate is reduced.

The efficiency of the collector was determined by considering the performance of the solar collector[8]. From the results in Fig. 17, it can

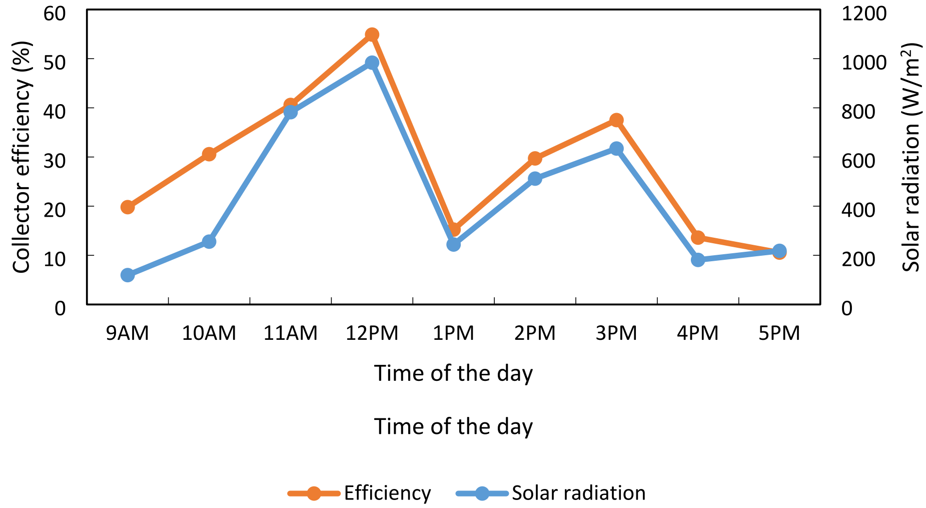

(c)

Fig. 17. (*continued*).

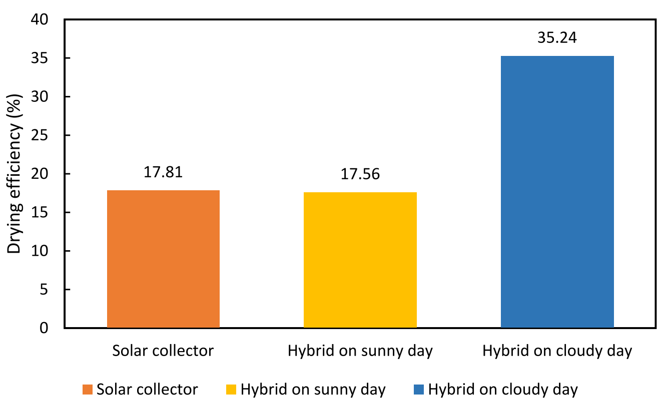

Fig. 18. Drying efficiency during drying of Citrus Hystrix leaves.

be observed that the efficiency of the collector during hybrid drying on the clear-sky day and the drying with the collector was higher than the efficiency during intermittent weather for both sets. Efficiency ranged between 32.25–58.97 % during hybrid drying on clear sky days, 28.65–59.34 % during collector only, and 10.55–54.9 % during hybrid drying in intermittent weather. The collector efficiency increased from 9 am to 12 am and was maintained until 1 am, except for intermittent weather due to increased incident solar radiation on the solar collector surface. The maximum instantaneous collector efficiency recorded was at 12 am on noon, which was 59.34 % (collector), 58.97 % (hybrid on clear sky day), and 54.9 % (hybrid on intermittent weather).

The drying efficiency for the drying process was calculated considering the amount of heat energy received by the solar collectors, the additional heat energy supplied by the auxiliary heater, and the electrical consumption of the ventilation fans[8]. The ability of the Citrus Hystrix leaves to dry was influenced by the temperature inside the chamber. Fig. 18 shows the efficiency of the process that uses the collector only for drying, hybrid drying under clear skies and during intermittent weather. The highest recorded drying efficiency was 35.24 % when using the hybrid system during intermittent weather, compared to the clear-sky day of 17.26 %. The auxiliary heater operated continuously during the drying process to support the heat production of the solar collector. The solar collector's efficiency was also 17.18 %, a reduction compared to the hybrid system. This result leads to a lower water removal rate from the surface of Citrus Hystrix leaves, subsequently causing a low drying efficiency.

4. Conclusions

The air temperature of the cylindrical solar drying chamber has a maximum temperature of 56.37 °C, the temperature of which is influenced by the varying solar radiation. The CFD results showed that the airflow and temperature distribution in the cylindrical drying chambers were uniform because of the curved surface of a cylinder, creating a smoother path for heated air to circulate combined with the slanted funnel. The drying air temperature in the hybrid drying system can be maintained between 45° C and 60° C with the implementation of the auxiliary heater. The hybrid setup significantly reduced the drying period to 4 h compared to 6.5 h using the purely solar collector mode. The hybrid system achieved the highest drying efficiency of 35.24 % during intermittent weather compared to the hybrid system on clear-sky days and using solar collectors at 17.26 % and 17.18 %, respectively. For future recommendations, further investigation of the influences of various factors on drying performance would be beneficial. These factors include the diameters and sizes of the chambers, the thickness of the walls, and the materials used in construction. Understanding these influences could lead to significant improvements in drying efficiency.

CRediT authorship contribution statement

M.A.A. Azmi: Writing – review & editing, Writing – original draft, Methodology, Investigation, Formal analysis. **A.A. Razak:** . **M.A.S.M. Tarminzi:** Writing – original draft, Methodology, Investigation, Formal analysis, Data curation. **A.F. Sharol:** Visualization, Validation, Resources, Project administration, Methodology. **A.S.M. Yudin:** Visualization, Validation, Supervision, Resources. **Z.A.A. Majid:** Validation, Resources, Methodology, Funding acquisition, Conceptualization.

Declaration of Competing Interest

The authors declare that they have no known competing financial interests or personal relationships that could have appeared to influence the work reported in this paper.

Acknowledgments

The authors wish to acknowledge Universiti Malaysia Pahang Al-Sultan Abdullah for financial support under project grant UIC241520 and RDU242717.

References

[1] M. Aktaş, A. Khanlari, B. Aktekeli, A. Amini, Analysis of a new drying chamber for heat pump mint leaves dryer, Int. J. Hydrogen Energy 42 (28) (2017) 18034–18044, https://doi.org/10.1016/j.ijhydene.2017.03.007.

[2] M.A.A. Azmi, A.A. Razak, M.A.S.M. Tarminzi, A.F. Sharol, A.S.M. Yudin, Z.A. A. Majid, Hydrodynamics Investigations of Kaffir Lime Leaves Drying in a Swirling Solar Drying Chamber with Inclined Slotted Angle Air Distributor, CFD Lett. 15 (2) (2023) 71–86, https://doi.org/10.37934/cfdl.15.2.7186.

[3] A.R. Celma, F. Cuadros, F. López-Rodríguez, Convective drying characteristics of sludge from treatment plants in tomato processing industries, Food Bioprod. Process. (2012), https://doi.org/10.1016/j.fbp.2011.04.003.

[4] P.C. Corrêa, F.M. Botelho, G.H.H. Oliveira, A.L.D. Goneli, O. Resende, S. de Carvalho Campos, Modelagem matemática do processo de secagem de espigas de milho, Acta Scientiarum - Agronomy 33 (4) (2011) 575–581, https://doi.org/10.4025/actasciagron.v33i4.7079.

[5] H. Essalhi, M. Benchrifa, R. Tadili, M.N. Bargach, Experimental and theoretical analysis of drying grapes under an indirect solar dryer and in open sun, Innov. Food Sci. Emerg. Technol. 49 (2018) 58–64, https://doi.org/10.1016/j.ifset.2018.08.002.

[6] M. Kumar, S.K. Sansaniwal, P. Khatak, Progress in solar dryers for drying various commodities, Renew. Sustain. Energy Rev. (2016), https://doi.org/10.1016/j.rser.2015.10.158.

[7] Moudakkar, T., El, Z., Vaudreuil, S., & Bounahmidi, T. (2020). Optimum design and performance analysis of heat exchanger coupling a fl ash dryer and parabolic trough collectors, *199*(September 2019), 152–163. https://doi.org/10.1016/j.solener.2020.02.024.

[8] S. Murali, P.R. Amulya, P.V. Alfiya, D.S.A. Delfiya, M.P. Samuel, Design and Performance Evaluation of Solar - LPG Hybrid Dryer for Drying of Shrimps, Renew. Energy (2019), https://doi.org/10.1016/j.renene.2019.10.002.

[9] M. Islam, M.I. Islam, M. Tusar, A.H. Limon, Effect of cover design on moisture removal rate of a cabinet type solar dryer for food drying application, Energy Procedia 160 (2018) (2019) 769–776, https://doi.org/10.1016/j.egypro.2019.02.181.

[10] S.M. Oliveira, T.R.S. Brandão, C.L.M. Silva, Influence of Drying Processes and Pretreatments on Nutritional and Bioactive Characteristics of Dried Vegetables: A Review, Food Eng. Rev. (2016), https://doi.org/10.1007/s12393-015-9124-0.

[11] R. Ouaabou, B. Nabil, M. Ouhammou, A. Idlimam, A. Lamharrar, S. Ennahli, M. Mahrouz, Impact of solar drying process on drying kinetics, and on bioactive profile of Moroccan sweet cherry, Renew. Energy 151 (2019) 908–918, https://doi.org/10.1016/j.renene.2019.11.078.

[12] S. Phoungchandang, W. Srinukroh, B. Leenanon, Citrus Hystrix leaf (Citrus hystric DC.) drying using tray and heat pump dehumidified drying, Drying Technol. 26 (12) (2008) 1602–1609, https://doi.org/10.1080/07373930802467490.

[13] P. Raksakantong, S. Siriamornpun, N. Meeso, Effect of drying methods on volatile compounds, fatty acids and antioxidant property of Thai Citrus Hystrix (Citrus hystrix D.C.), Int. J. Food Sci. Technol. (2012), https://doi.org/10.1111/j.1365-2621.2011.02883.x.

[14] K. Sacilik, A.K. Elicin, The thin layer drying characteristics of organic apple slices, J. Food Eng. (2006), https://doi.org/10.1016/j.jfoodeng.2005.03.024.

[15] M. Yahya, A. Fudholi, K. Sopian, Energy and exergy analyses of solar-assisted fluidized bed drying integrated with biomass furnace, Renew. Energy 105 (2017) 22–29, https://doi.org/10.1016/j.renene.2016.12.049.

[16] A.F. Sharol, A. Abdul Razak, Z.A. Abdul Majid, A. Fudholi, Experimental study on performance of square tube absorber with phase change material, Int. J. Energy Res. 44 (2) (2020) 1000–1011, https://doi.org/10.1002/er.4971.

[17] A.F. Sharol, A.A. Razak, Z.A.A. Majid, M.A.A. Azmi, M.A.S.M. Tarminzi, Performance of force circulation cross-matrix absorber solar heater integrated with latent heat energy storage material, IOP Conference Series: Materials Science and Engineering 469 (1) (2019), https://doi.org/10.1088/1757-899X/469/1/012107.

[18] M. Sandali, A. Boubekri, D. Mennouche, N. Gherraf, Improvement of a direct solar dryer performance using a geothermal water heat exchanger as supplementary energetic supply. An experimental investigation and simulation study, Renew. Energy 135 (2019) 186–196, https://doi.org/10.1016/j.renene.2018.11.086.

[19] S. Suherman, N.F. Azaria, S. Karami, Performance Study of Fluidized Bed Dryer with Immersed Heater for Paddy Drying, IOP Conference Series: Materials Science and Engineering 316 (1) (2018), https://doi.org/10.1088/1757-899X/316/1/012026.

[20] S. Suherman, H. Widuri, S. Patricia, E.E. Susanto, R.J. Sutrisna, Energy analysis of a hybrid solar dryer for drying coffee beans, International Journal of Renewable Energy Development 9 (1) (2020) 131–139, https://doi.org/10.14710/ijred.9.1.131-139.

[21] S.M. Tasirin, S.K. Kamarudin, J.A. Ghani, K.F. Lee, Optimisation of drying parameters of bird's eye chilli in a fluidised bed dryer, J. Food Eng. (2007), https://doi.org/10.1016/j.jfoodeng.2006.06.030.

[22] S.M. Tasirin, I. Puspasari, A.W. Lun, P.V. Chai, W.T. Lee, Drying of Citrus Hystrix leaves in a fluidised bed dryer with inert particles: Kinetics and quality determination, Ind. Crop. Prod. 61 (2014) 193–201, https://doi.org/10.1016/j.indcrop.2014.07.004.

[23] Saini, Raj Kumar, Devender Kumar Saini, Rajeev Gupta, Piush Verma, Robin Thakur, Sushil Kumar, and Ali wassouf. 2023. "Technological Development in Solar Dryers from 2016 to 2021-A Review." *Renewable and Sustainable Energy Reviews* 188 (October). https://doi.org/10.1016/j.rser.2023.113855.

[24] R. Trostle, A Report from the Economic Research Service Global Agricultural Supply and Demand : Factors Contributing to the Recent Increase in Food. *Agricultural*, Outlook (2008).

[25] E. Vengadesan, R. Senthil, A review on recent development of thermal performance enhancement methods of flat plate solar water heater, Sol. Energy 206 (June) (2020) 935–961, https://doi.org/10.1016/j.solener.2020.06.059.

[26] Y. Wang, X. Li, X. Chen, B. Li, X. Mao, J. Miao, W. Gao, Effects of hot air and microwave-assisted drying on drying kinetics, physicochemical properties, and energy consumption of chrysanthemum, Chem. Eng. Process. - Process Intesif. 129 (2018) 84–94, https://doi.org/10.1016/j.cep.2018.03.020.

[27] Wengang Hao, Shuonan Liu, B. M. and Y. L. (2020). Mathematical Modeling and Performance Analysis of a New Hybrid Solar Dryer of Lemon Slices for.

[28] T.A. Yassen, H.H. Al-kayiem, Experimental Investigation and Evaluation of Hybrid Solar / Thermal Dryer Combined with Supplementary Recovery Dryer 134 (2016) 284–293.

[29] H.H. Al-Kayiem, A.A. Gitan, Flow Uniformity Assessment in a Multi-Chamber Cabinet of a Hybrid Solar Dryer, Sol. Energy 224 (June) (2021) 823–832, https://doi.org/10.1016/j.solener.2021.06.058.

[30] R. Castilla, P.J. Gamez-Montero, N. Ertrk, A. Vernet, M. Coussirat, E. Codina, Numerical simulation of turbulent flow in the suction chamber of a gearpump using deforming mesh and mesh replacement, Int. J. Mech. Sci. 52 (2010) 1334–1342.

[31] H. Bhavsar, C.M. Patel, Performance analysis of cabinet type solar dryer for ginger drying with & without thermal energy storage material, Mater. Today:. Proc. 73 (2023) 595–603, https://doi.org/10.1016/j.matpr.2022.11.280.

[32] Razak, A A, Z A A Majid, W H Azmi, M H Ruslan, Sh Choobchian, G Naja, and others, 'Review on Matrix Thermal Absorber Designs for Solar Air Collector', 64 (2016), 682–93 <https://doi.org/10.1016/j.rser.2016.06.015>.

[33] M.A.S.M. Tarminzi, A.A. Razak, M.A.A. Azmi, A. Fazlizan, Z.A.A. Majid, K. Sopian, Comparative Study on Thermal Performance of Cross-Matrix Absorber Solar Collector with Series and Parallel Configurations, Case Studies in Thermal Engineering 25, no. February (2021) 100935, https://doi.org/10.1016/j.csite.2021.100935.